Criticalities in the itinerant ferromagnet UGe$_2$

Marcin M. Wysokiński,[1,*] Marcin Abram,[1,†] and Józef Spałek[1,2,‡]

[1]*Marian Smoluchowski Institute of Physics, Jagiellonian University, Łojasiewicza 11, PL-30-348 Kraków, Poland*
[2]*Academic Centre for Materials and Nanotechnology (ACMiN), AGH University of Science and Technology, Al. Mickiewicza 30,*
PL-30-059 Kraków, Poland

We provide a microscopic description of the magnetic properties of UGe$_2$ and, in particular, of its both classical and quantum critical behavior. Namely, we account for all the critical points: the critical ending point (CEP) at the metamagnetic phase transition, the tricritical point, and the quantum critical end point at the ferromagnetic to paramagnetic phase transition. Their position agrees quantitatively with experiment. Additionally, we predict that the metamagnetic CEP can be traced down to zero temperature and becomes quantum critical point by a small decrease of both the total electron concentration and the external pressure. The system properties are then determined by the quantum critical fluctuations appearing near the instability point of the Fermi surface topology.

Introduction. Attempts to determine the quantum critical behavior and the corresponding critical points (QCPs) have attracted much attention due to the unique phenomena with singular physical properties associated with them as temperature $T \rightarrow 0$ and other parameters (pressure p, applied field H, or electron concentration n) are varied [1–3]. Additionally, in the canonical case—the heavy fermion systems—unconventional superconductivity often appears near those QCPs making the quantum critical fluctuations the primary pairing inducing factor. Also, the classical critical points (CCPs) and their evolution towards QCP provide the testing ground for study of detailed quantitative behavior of different systems [4,5].

UGe$_2$, in this respect, is one of the unique materials that exhibit all the above features. Therefore, the explanation of the magnetic phase diagram and intimately connected critical points within a single theoretical framework would provide a complete understanding of this remarkable quantum material [4,6–9]. The phase diagram on the pressure-temperature (p-T) plane comprises two ferromagnetic phases, of weaker (FM1) and stronger (FM2) magnetization, paramagnetic phase (PM), as well as the spin-triplet superconducting phase (SC) [4,6,10]. SC disappears at the same pressure as FM [6] and the maximum of the superconducting critical temperature T_s coincides with the critical pressure for the FM2-FM1 phase transition [7]. Thus, it is strongly suggestive that FM and SC are strongly intertwined as described by some theoretical approaches [11–15].

The p-T-H phase diagram for UGe$_2$ comprises the characteristic *wing shape* [8,9]. Such structure was theoretically obtained by Belitz *et al.* [16] within mean-field approach for a single-band itinerant ferromagnet. However, this approach cannot account for the two different ferromagnetic phases appearing in UGe$_2$, as well as for the critical ending point (CEP), separating the region with a discontinuous drop in magnetization from a crossover regime [8,17].

In this work we provide a quantitative microscopic description of all magnetic critical properties of UGe$_2$ within the framework of the Anderson lattice model (ALM) treated by a modified Gutzwiller approach [18], called *the statistically consistent Gutzwiller approximation* (SGA) (for a description of the method and a detailed comparison to the slave-boson approach, see Ref. [19]; for its applications, see Refs. [20]). Validity of this model in the context of UGe$_2$ [18] is based on earlier results: first, on band structure calculations [21,22] and second, on experimental observations [4,6,23]. The first feature is a quasi-two-dimensional topology of the Fermi surface (FS) [21,22] which justifies calculations for a two-dimensional square lattice. On the other hand, despite the circumstance that the distance between uranium atoms is above the Hill limit [4], the experimental value of the paramagnetic moment per U atom is different from that for either f^3 or f^2 configurations [6,24]. This speaks for the presence of a sizable hybridization between the initially localized f electrons and those from the conduction band. For strong enough hybridization, f electrons contribute essentially to the heavy itinerant quasiparticle states and play a dominant role in the magnetic properties [6,10,24].

We provide a coherent explanation of FM and PM phase appearances as driven by a competition between the hybridization from one side and the f-f Coulomb local repulsive interaction from the other [18]. Specifically, we obtain two different FM phases [15,18,25–28] by varying the predetermined position of the chemical potential with respect to the peaks in the quasiparticle density of states (DOS) including the spin-split subbands. Although, Gutzwiller ansatz in certain regimes favors antiferromagnetism over FM [25–27,29,30], we restrict our discussion to the latter phase, because in the considered range of electron concentration, $n \simeq 1.6$, FM phase turned out to have the lowest energy [25,26].

In Fig. 1 we draw schematically the respective DOS for considered phases. It can be seen clearly that the shape of the FS (limiting the filled parts) will be vastly different in each of the phases. Within our approach, most of the properties of UGe$_2$ at $T = 0$ can be explained [18] in agreement with related experiments of magnetization [7], neutron scattering [10,24], and the de Haas–van Alphen oscillations [31,32]. The character of the FM1 phase, which we obtain as a half-metallic type [cf. Fig. 1(b)], is also supported by the band-structure calculations [22].

In the present work we extend our previous approach [18] to nonzero temperature and on this basis we determine the

————————
*marcin.wysokinski@uj.edu.pl
†marcin.abram@uj.edu.pl
‡ufspalek@if.uj.edu.pl

character of all phase transitions on the p-T-H diagram of UGe$_2$, as well as discuss the nature of all the classical and quantum critical points. We also show that by a small decrease of electron concentration (by $\sim 7\%$), the system can reach another quantum criticality via a metamagnetic transition upon changing the pressure. We also predict the corresponding change in FS topology distinguishing the two phases of significantly different magnetic susceptibility.

Model. We start from ALM with the Zeeman term included ($h \equiv \frac{1}{2}g\mu_0\mu_B H$) in the Hamiltonian

$$\hat{\mathcal{H}} - \mu\hat{N} = \sum_{\mathbf{i},\mathbf{j},\sigma}' t_{\mathbf{ij}}\hat{c}^\dagger_{\mathbf{i},\sigma}\hat{c}_{\mathbf{j},\sigma} - \sum_{\mathbf{i},\sigma}(\mu + \sigma h)\hat{n}^c_{\mathbf{i},\sigma}$$
$$+ \sum_{\mathbf{i},\sigma}(\epsilon_f - \mu - \sigma h)\hat{n}^f_{\mathbf{i},\sigma} + U\sum_{\mathbf{i}}\hat{n}^f_{\mathbf{i},\uparrow}\hat{n}^f_{\mathbf{i},\downarrow}$$
$$+ V\sum_{\mathbf{i},\sigma}(\hat{f}^\dagger_{\mathbf{i},\sigma}\hat{c}_{\mathbf{i},\sigma} + \hat{c}^\dagger_{\mathbf{i},\sigma}\hat{f}_{\mathbf{i},\sigma}), \quad (1)$$

which comprises dispersive conduction (c) band electrons and f electrons coming from atomic f shell located at $\epsilon_f < 0$. In the model we include specifically the nearest- ($t < 0$) and the second-nearest- ($t' = 0.25|t|$) neighbor hopping amplitudes between c electrons, f level at $\epsilon_f = -3|t|$, sizable $f - f$ Coulomb repulsion $U = 5|t|$, and the $c - f$ hybridization V of the on-site form.

To obtain an effective single particle picture from the many-body Hamiltonian (1) we use the extended Gutzwiller approximation (GA) called the SGA (for details, see [19]). The method was successfully applied to a number of problems [20]. Formally, we add to the effective Hamiltonian obtained in GA [33,34], $\hat{\mathcal{H}}_{GA}$, additional constraints on the number of f electrons and their magnetization by means of the Lagrange multipliers. It leads to the new effective Hamiltonian $\hat{\mathcal{H}}_{SGA}$ of the form

$$\hat{\mathcal{H}}_{SGA} \equiv \hat{\mathcal{H}}_{GA} - \lambda^f_n\left(\sum_{\mathbf{k},\sigma}\hat{n}^f_{\mathbf{k},\sigma} - \Lambda n_f\right) - \lambda^f_m\left(\sum_{\mathbf{k},\sigma}\sigma\hat{n}^f_{\mathbf{k},\sigma} - \Lambda m_f\right)$$

$$\equiv \sum_{\mathbf{k},\sigma}\hat{\Psi}^\dagger_{\mathbf{k}\sigma}\begin{pmatrix} \epsilon^c_{\mathbf{k}} - \sigma h - \mu & \sqrt{q_\sigma}V \\ \sqrt{q_\sigma}V & \epsilon_f - \sigma(h + \lambda^f_m) - \lambda^f_n - \mu \end{pmatrix}\hat{\Psi}_{\mathbf{k}\sigma} + \Lambda\left(Ud^2 + \lambda^f_n n_f + \lambda^f_m m_f\right), \quad (2)$$

where $\hat{\Psi}^\dagger_{\mathbf{k}\sigma} \equiv (\hat{c}^\dagger_{\mathbf{k},\sigma}, \hat{f}^\dagger_{\mathbf{k},\sigma})$. Furthermore, q_σ is the hybridization narrowing factor in the standard form [18,20], and Λ is a number of lattice sites.

At nonzero temperature, one needs to minimize the generalized Landau grand-potential functional

$$\frac{\mathcal{F}}{\Lambda} = -\frac{1}{\Lambda\beta}\sum_{\mathbf{k}\sigma b}\ln\left[1 + e^{-\beta E^b_{\mathbf{k}\sigma}}\right]$$
$$+ \left(\lambda^f_n n_f + \lambda^f_m m_f + Ud^2\right), \quad (3)$$

where $E^b_{\mathbf{k}\sigma}$ are four eigenvalues of the effective Hamiltonian (2) labeled with the spin (σ) and band (b) indices. λ^f_n and λ^f_m are the Lagrange multipliers assuring the correct statistical consistency of equations for n_f and m_f and play the role of correlation-induced effective fields [20]. Minimization of $\mathcal{F}$ is carried out with respect to the set of all parameters $\vec{\lambda} \equiv \{d, n_f, m_f, \lambda^f_n, \lambda^f_m\}$. Additionally, as the number of particles in the system is conserved we have to determine the chemical potential and adjust it to each of the phases according to the condition $n = 1/\Lambda\sum_{\mathbf{k}b\sigma}f(E^b_{\mathbf{k}\sigma})$, with $f(E)$ being the Fermi-

Dirac function. In effect, the model is described by set of six algebraic equations which are solved with the help of the GSL library, with typical accuracy 10^{-11}.

The Landau grand-potential functional for the equilibrium values of the parameters, $\mathcal{F}_0$, has the meaning of the physical grand potential Ω which is the proper quantity for studying the system at any temperature, $\mathcal{F}_0 \equiv \Omega \equiv U - TS - \mu N$. Therefore, the free energy of the system is defined by $F = \mathcal{F}_0 + \mu N$ and the ground-state energy is $E_G \equiv F(T = 0)$.

Results. We assume that the main effect of the applied pressure is emulated by an increase of the hybridization amplitude $|V|$, even though other parameters (e.g., ϵ_f) may also change. However, as our previous results indicate, hybridization change is the principal factor of the pressure dependencies observed in UGe$_2$ [18].

In Fig. 2 we plot the phase diagram on the $|V| - T$ plane. In the low-T regime we are able to reproduce the correct evolution of both metamagnetic (left) and ferromagnetic to paramagnetic (right) phase transitions observed in experiment (cf. inset), together with the respective critical behavior [7–9,17]. The position of the CCPs is very sensitive to the selected total band filling, $n = n_f + n_c$. Our fitting constraint is the ratio of the corresponding critical temperatures, $T_{CEP}/T_{TCP} \approx 7$ K/24 K [8]. Consequently, for the band filling $n = 1.6$, selected in our previous analysis at $T = 0$ [18], we obtain agreement of our calculated ratio under the proviso that experimental values of the critical temperatures are determined with accuracy ± 0.25 K.

Our model does not account for correct curvatures of phase transitions above CCPs (cf. Fig. 2). This discrepancy can be attributed to the fact that also other microscopic parameters can alter when applying pressure, e.g., ϵ_f, and to additional
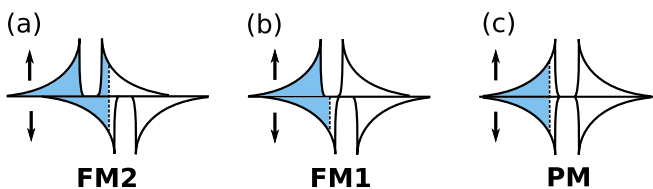

FIG. 1. (Color online) Schematic characterization of phases by their spin-resolved density of states. The arrows label the spin subbands and the dotted line marks the position of the chemical potential.
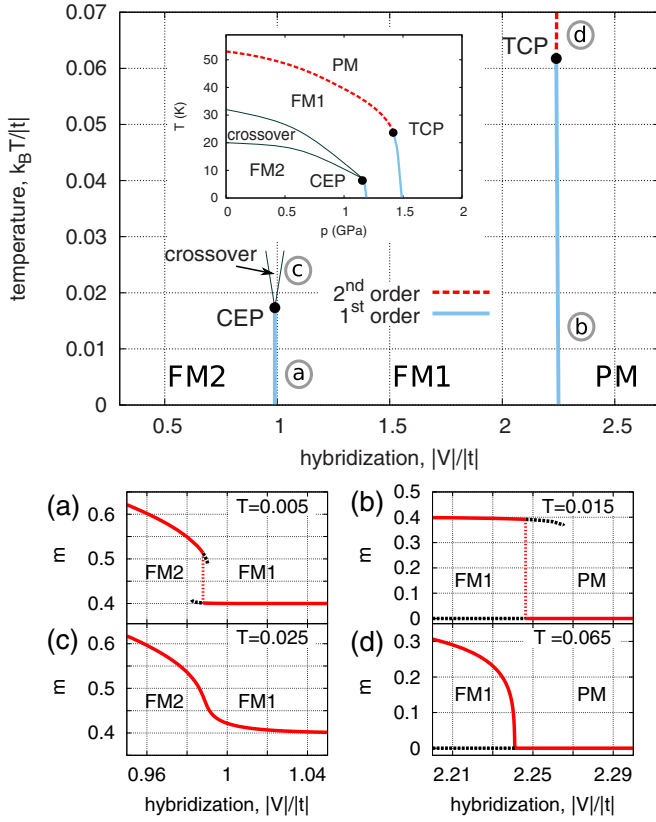
FIG. 2. (Color online) Top: Phase diagram on hybridization strength-reduced temperature plane encompassing both FM and PM phases for total band filling $n = 1.6$. The correct character of phase transitions and positions of critical points in UGe$_2$ [7–9,17] is reproduced. For comparison, we present in the inset the experimental p-T phase diagram of UGe$_2$ (cf. [7,8]). In (a)–(d) we draw the magnetization change with the increasing hybridization strength when the system undergoes phase transition at points indicated with respective encircled letters (a)–(d). Solid red lines denote energetically favorable solution, whereas dashed black lines denote the unstable solutions.
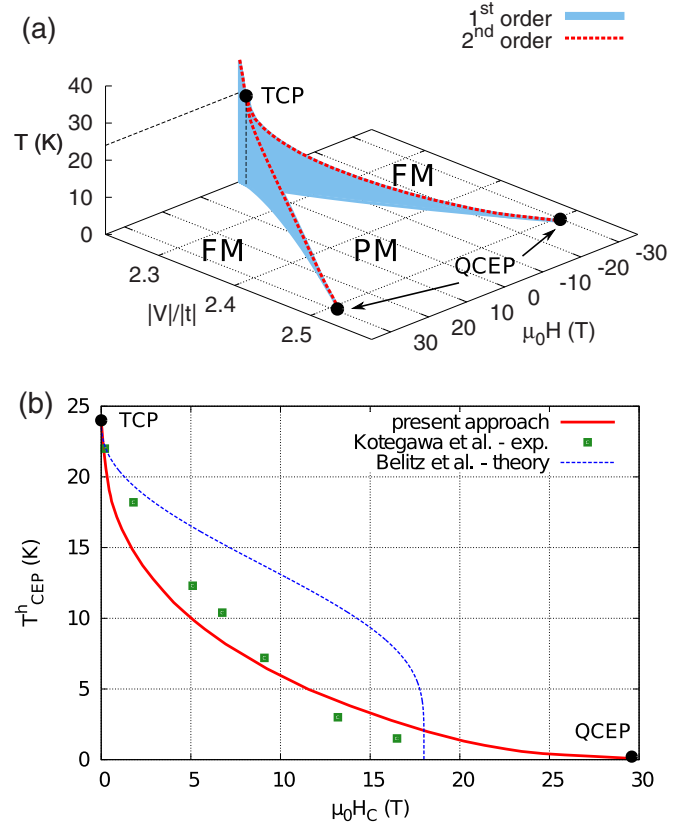

FIG. 3. (Color online) (a) Wing structure of the phase transition planes derived from our model. (b) Comparison of the calculated dependence of the temperature vs applied magnetic field at the critical end point (CEP) with the experimental points adopted from [9]. For comparison, we include also the prediction by Belitz *et al.* [16], with the fitting parameters selected on the basis [9]: $H_{\mathrm{QCEP}} = 18$ T and $T_{\mathrm{TCP}} = 24$ K.

entropic factors important in the case of $T > 0$ Gutzwiller projection [35,36].

In our calculations we have used reduced temperature $k_B T/|t|$. We rescale it to the physical units by relating it to the experimentally measured values at CCPs [7–9,17]. Accordingly, we also rescale the reduced field $\frac{1}{2} g \mu_B \mu_0 H/|t|$ to Tesla units.

At the metamagnetic (FM2-FM1) phase transition we obtain CEP separating the discontinuous-transition line from the crossover regime. At low T both solutions with the weaker and the stronger magnetization coexist in the limited range of the hybridization strength [cf. Fig. 2(a)]. As the system approaches the transition from the FM1 side, FS changes drastically only in one spin subband, in which the chemical potential crosses the hybridization gap, resulting also in a discontinuous jump of the total moment $m = m_f + m_c$. With the increasing temperature, the edges of the gap are gradually smeared out. This leads to a deviation from the pure half-metallic type of the FM1 phase. The magnetization is *bending* towards the trend observed in the FM2 phase,

and eventually at CEP it is changing to a crossover line [cf. Fig. 2(c)].

In the case of FM to PM transition the situation is different [cf. Figs. 2(b) and 2(d)]. At low temperature, the magnetization of this *half-metallic* FM1 phase discontinuously drops to zero [cf. Fig. 2(b)]. However, with the increasing temperature, the ferromagnetic solution departs from a sharp half-metallic type and slowly *bends* over towards the paramagnetic solution, eventually reaching the critical point by changing the transition character to that of second order [cf. Fig. 2(d)]. The just described critical point is of tricritical character (TCP). This is because its evolution can be followed by applying the magnetic field down to $T = 0$, where it turns into the quantum critical ending point (QCEP) [cf. Fig. 3(a)]. In this manner, we have achieved a full characteristic at the *wing-shape p-T-H* phase diagram [8,9]. As the detailed form of the hybridization change with applied pressure is unknown, and in principle nonlinear, we compare our predicted shape of wings by tracing the evolution of CEP on the temperature-magnetic field T_{CEP}^h-$\mu_0 H_C$ plane [cf. Fig. 3(b)] and comparing it to the experimental data [9]. We obtain a satisfactory quantitative agreement with the experimental points, as well as recover its proper curvature. For comparison, the results from the
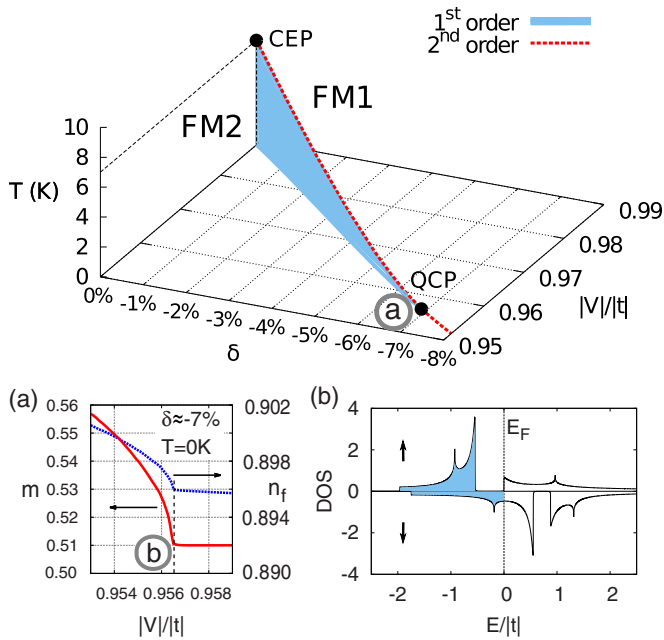
FIG. 4. (Color online) Top: Evolution of CEP on the $|V|$-T-δ plane down to $T = 0$ and QCP (see main text). Bottom: (a) Change of magnetization and f electron number as the system undergoes quantum critical transition. (b) Density of states at QCP. Note the intermediate character of FS between FM2 and FM1 of the state at QCP. Encircled letter ⓐ at top diagram refers to the position of the curves in panel (a), and respectively ⓑ at panel (a) to the position of the DOS in (b).

mean-field approach to the single-band case by Belitz *et al.* [16] are also drawn, as is universal explanation of tricritical behavior of itinerant ferromagnets. Nevertheless, as suggested by the authors in Ref. [9], the crucial element determining for UGe$_2$ the correct shape of the wings is the change of FS, present in our two-band ALM model. We also predict that the curve of the T_{CEP}^h vs $\mu_0 H_C$ dependence has a longer tail than that estimated in Ref. [9], i.e., that QCEP should be located at fields around 30 T. Our estimate thus calls for a more precise determination of the QCEP position.

In fitting to the data in Fig. 3 we have assumed that the g factor for f electrons $g_f = 2$ (the same as for c electrons). This assumption is based on the presumption that for itinerant electrons the crystal-field multiplet structure is washed out. Parenthetically, taking g_f significantly different provides a worse agreement, but the curvature character remains unchanged.

In Fig. 4 we draw the evolution of CEP at the metamagnetic transition with the decrease of both the hybridization and the electron concentration. The latter quantity is characterized by the parameter $\delta = \frac{n_x-n}{n}100\%$, where $n = 1.6$ is initial and n_x is the actual concentration. On the V-T-δ phase diagram the CEP can be followed down to zero temperature, where it joins the second-order transition line [cf. Fig. 4(a)]. At this second-order transition the Fermi level for the majority spin subband is exactly at the border of the gap [cf. Fig. 4(b)]. It means that along this line quantum critical fluctuations of FS topology are present. In other terms, we have a strong indication that in the vicinity of the SC dome maximum this compound exhibits a *Lifshitz* type of quantum critical behavior. This quantum critical transition can be associated also with the specific valence change [cf. Fig. 4(a)]. However, here the average f electron number changes continuously in contrast to the discontinuous drop originating from the f-c electron repulsion [37]. The difference in the origin of *Lifshitz* type of ferromagnetic QCP with respect to that considered before [38,39] is that here it results from the two-band model and separates different FM phases.

Summary. We have described the phase diagram of UGe$_2$ at nonzero temperature and have determined the location of the critical points, as well as proposed an additional quantum critical point for UGe$_2$. With the help of the Anderson lattice model we are able to reproduce quantitatively all the principal features of the magnetism in this compound. We also have determined the location of experimentally observed critical and quantum critical points, together with a correct order of the phase transitions related to them.

Although our mean-field approach seems to capture all the features concerning details of the p-T-H phase diagram of UGe$_2$, we should note that, in principle, fluctuations of order parameters can bring quantitative changes to our results. However, as the phase transitions are induced by the drastic changes of the Fermi surface, the effect of the fluctuations should be minor (except near the predicted QCP—cf. Fig. 4) and may lead to a correction of the CEP and TCP positions.

It should be noted that we have employed an orbitally nondegenerate ALM. Accounting for the degenerate one would imply inclusion of the residual Hund's rule interaction present in the degenerate ALM model which could be important in inducing the spin-triplet pairing [40].

[1] H. v. Löhneysen, A. Rosch, M. Vojta, and P. Wölfle, Rev. Mod. Phys. **79**, 1015 (2007).

[2] Q. Si, P. Gegenwart, and F. Steglich, *Understanding Quantum Phase Transitions*, edited by L. D. Carr (CRC Press, Boca Raton, 2011), Chaps. 8, 18, pp. 193–216, 445–468.

[3] A. Ślebarski and J. Spałek, Phys. Rev. Lett. **95**, 046402 (2005).

[4] C. Pfleiderer, Rev. Mod. Phys. **81**, 1551 (2009) (Sec. III.A).

[5] J. Spalek, A. Datta, and J. M. Honig, Phys. Rev. Lett. **59**, 728 (1987); J. Spałek, Phys. Status Solidi B **243**, 78 (2006).

[6] S. S. Saxena, P. Agarwal, K. Ahilan, F. M. Grosche, R. K. W. Haselwimmer, M. J. Steiner, E. Pugh, I. R. Walker, S. R. Julian, P. Monthoux, G. G. Lonzarich, A. Huxley, I. Sheikin, D. Braithwaite, and J. Flouquet, Nature (London) **406**, 587 (2000).

[7] C. Pfleiderer and A. D. Huxley, Phys. Rev. Lett. **89**, 147005 (2002).

[8] V. Taufour, D. Aoki, G. Knebel, and J. Flouquet, Phys. Rev. Lett. **105**, 217201 (2010).

[9] H. Kotegawa, V. Taufour, D. Aoki, G. Knebel, and J. Flouquet, J. Phys. Soc. Jpn. **80**, 083703 (2011).

[10] A. Huxley, I. Sheikin, E. Ressouche, N. Kernavanois, D. Braithwaite, R. Calemczuk, and J. Flouquet, Phys. Rev. B **63**, 144519 (2001).

[11] T. R. Kirkpatrick, D. Belitz, T. Vojta, and R. Narayanan, Phys. Rev. Lett. **87**, 127003 (2001).

[12] K. Machida and T. Ohmi, Phys. Rev. Lett. **86**, 850 (2001).

[13] A. A. Abrikosov, J. Phys: Condens. Matter **13**, L943 (2001).

[14] D. Sa, Phys. Rev. B **66**, 140505 (2002).

[15] K. G. Sandeman, G. G. Lonzarich, and A. J. Schofield, Phys. Rev. Lett. **90**, 167005 (2003).

[16] D. Belitz, T. R. Kirkpatrick, and J. Rollbühler, Phys. Rev. Lett. **94**, 247205 (2005).

[17] F. Hardy, C. Meingast, V. Taufour, J. Flouquet, H. v. Löhneysen, R. A. Fisher, N. E. Phillips, A. Huxley, and J. C. Lashley, Phys. Rev. B **80**, 174521 (2009).

[18] M. M. Wysokiński, M. Abram, and J. Spałek, Phys. Rev. B **90**, 081114(R) (2014).

[19] J. Jędrak, J. Kaczmarczyk, and J. Spałek, arXiv:1008.0021.

[20] J. Jędrak and J. Spałek, Phys. Rev. B **83**, 104512 (2011); J. Kaczmarczyk and J. Spałek, *ibid.* **84**, 125140 (2011); O. Howczak, J. Kaczmarczyk, and J. Spałek, Phys. Status Solidi B **250**, 609 (2013); A. P. Kądzielawa, J. Spałek, J. Kurzyk, and W. Wójcik, Eur. Phys. J. B **86**, 252 (2013); M. Abram, J. Kaczmarczyk, J. Jędrak, and J. Spałek, Phys. Rev. B **88**, 094502 (2013); M. Zegrodnik, J. Spałek, and J. Bünemann, New J. Phys. **15**, 073050 (2013); M. M. Wysokiński and J. Spałek, J. Phys.: Condens. Matter **26**, 055601 (2014).

[21] A. B. Shick and W. E. Pickett, Phys. Rev. Lett. **86**, 300 (2001).

[22] M. Samsel-Czekała, M. Werwiński, A. Szajek, G. Chełkowska, and R. Troć, Intermetallics **19**, 1411 (2011).

[23] V. H. Tran, S. Paschen, R. Troć, M. Baenitz, and F. Steglich, Phys. Rev. B **69**, 195314 (2004).

[24] N. Kernavanois, B. Grenier, A. Huxley, E. Ressouche, J. P. Sanchez, and J. Flouquet, Phys. Rev. B **64**, 174509 (2001).

[25] R. Doradziński and J. Spałek, Phys. Rev. B **56**, R14239 (1997).

[26] R. Doradziński and J. Spałek, Phys. Rev. B **58**, 3293 (1998).

[27] O. Howczak and J. Spałek, J. Phys: Condens. Matter **24**, 205602 (2012).

[28] K. Kubo, Phys. Rev. B **87**, 195127 (2013).

[29] G. Kotliar and A. E. Ruckenstein, Phys. Rev. Lett. **57**, 1362 (1986).

[30] V. Dorin and P. Schlottmann, Phys. Rev. B **46**, 10800 (1992).

[31] T. Terashima, T. Matsumoto, C. Terakura, S. Uji, N. Kimura, M. Endo, T. Komatsubara, and H. Aoki, Phys. Rev. Lett. **87**, 166401 (2001).

[32] R. Settai, M. Nakashima, S. Araki, Y. Haga, T. C. Kobayashi, N. Tateiwa, H. Yamagami, and Y. Onuki, J. Phys: Condens. Matter **14**, L29 (2002).

[33] T. M. Rice and K. Ueda, Phys. Rev. Lett. **55**, 995 (1985).

[34] P. Fazekas and B. H. Brandow, Phys. Scr. **36**, 809 (1987).

[35] W.-S. Wang, X.-M. He, D. Wang, Q.-H. Wang, Z. D. Wang, and F. C. Zhang, Phys. Rev. B **82**, 125105 (2010).

[36] M. Sandri, M. Capone, and M. Fabrizio, Phys. Rev. B **87**, 205108 (2013).

[37] K. Miyake and S. Watanabe, J. Phys. Soc. Jpn. **83**, 061006 (2014).

[38] R. Roussev and A. J. Millis, Phys. Rev. B **63**, 140504 (2001).

[39] D. Fay and J. Appel, Phys. Rev. B **22**, 3173 (1980).

[40] M. Zegrodnik, J. Bünemann, and J. Spałek, New J. Phys. **16**, 033001 (2014); J. Spałek and M. Zegrodnik, J. Phys.: Condens. Matter **25**, 435601 (2013).